vpu Transmembrane Peptide Structure Obtained by Site-Specific Fourier Transform Infrared Dichroism and Global Molecular Dynamics Searching

Andreas Kukol and Isaiah T. Arkin
Cambridge Center for Molecular Recognition, Department of Biochemistry, University of Cambridge, Cambridge CB2 1GA, England

ABSTRACT The recently developed method of site-directed Fourier transform infrared dichroism for obtaining orientational constraints of oriented polymers is applied here to the transmembrane domain of the *vpu* protein from the human immunodeficiency virus type 1 (HIV-1). The infrared spectra of the 31-residue-long *vpu* peptide reconstituted in lipid vesicles reveal a predominantly α-helical structure. The infrared dichroism data of the ^{13}C-labeled peptide yielded a helix tilt $\beta = (6.5 \pm 1.7)°$ from the membrane normal. The rotational pitch angle ω, defined as zero for a residue located in the direction of the helix tilt, is $\omega = (283 \pm 11)°$ for the ^{13}C labels Val^{13}/Val^{20} and $\omega = (23 \pm 11)°$ for the ^{13}C labels Ala^{14}/Val^{21}. A global molecular dynamics search protocol restraining the helix tilt to the experimental value was performed for oligomers of four, five, and six subunits. From 288 structures for each oligomer, a left-handed pentameric coiled coil was obtained, which best fits the experimental data. The structure reveals a pore occluded by Trp residues at the intracellular end of the transmembrane domain.

INTRODUCTION

The structural determination of membrane proteins is still a difficult task for x-ray crystallography and solution NMR methods. The transmembrane domains of ion channels have been approached by molecular modeling (Sansom, 1998; Sansom et al., 1998). In these cases, orientational information combined with a global molecular dynamics (MD) search can be used to obtain a highly reliable structural model (Kukol et al., 1999). Fourier transform infrared (FTIR) spectroscopy has been shown to be a useful tool for secondary structural determination of proteins (Byler and Susi, 1986) and monitoring even subtle conformational changes in bacteriorhodopsin (Torres et al., 1995; Cladera et al., 1996). In this work we have used the recently developed method of site-specific infrared dichroism (Arkin et al., 1997) to obtain the transmembrane helix tilt and the rotation angles of specific residues about the helix axis for the HIV-1 *vpu* protein.

The 81-residue *vpu* protein belongs to the auxiliary proteins of the human immunodeficiency virus type 1 (HIV-1) (Cohen et al., 1988; Strebel et al., 1988). It is composed of an N-terminal domain, where residues 1–5 are probably extracellular; a 22-residue segment that spans the membrane; and the cytoplasmic C-terminal domain (Maldarelli et al., 1993). *vpu* forms homooligomers of at least four subunits, as detected by gel electrophoresis (Maldarelli et al., 1993). The C-terminal cytoplasmic domain is responsible for the degradation of one of the HIV-1 coreceptor molecules, CD4 (Schubert et al., 1996a; Schubert and Strebel, 1994), allowing the *env* glycoprotein to be transported to the cell surface. The N-terminal domain is responsible for virus particle release (Schubert et al., 1996a), but the molecular basis of these actions is unknown. It has been shown that phosphorylation of the cytoplasmic domain is essential for CD4 degradation, although it is not absolutely required for virus particle release (Friborg et al., 1995; Schubert et al., 1996a; Schubert and Strebel, 1994). Virus particle release is not specific to HIV-1, because *vpu* is capable of enhancing the particle release of different retroviruses (Gottlinger et al., 1993; Xiao Jian et al., 1992).

The transmembrane domain has been studied independently of the cytoplasmic domain. By analogy with the *M2* protein of *Influenza* A virus (Lamb and Pinto, 1997), it has been suggested that the transmembrane part of *vpu* may act as an ion channel (Klimkait et al., 1990; Maldarelli et al., 1993; Schubert and Strebel, 1994; Strebel et al., 1989). In fact, ion channel activity for monovalent cations has been observed in *Xenopus* oocytes and in planar lipid bilayers (Schubert et al., 1996b; Ewart et al., 1996). Recently, however, controversial results have been reported. *vpu* expression in oocytes reduces basal membrane conductance (Coady et al., 1998), whereas *vpu* expression in *Escherichia coli* and eukaryotic COS cells enhances membrane permeability to charged molecules (Gonzales and Carrasco, 1998).

The method of site-specific infrared dichroism (Arkin et al., 1997) combined with a global MD search has recently yielded a structure for the tetrameric influenza *M2*-H^+ channel that is not only in accordance with NMR data, but is also consistent with results obtained by the use of mutagenesis that are available in the literature (e.g., Holsinger et al., 1994). Because the oligomerization number of *vpu* is not known, we extend the method, first by undertaking the MD search for different oligomerization states, as the orientational data are independent of the helix oligomerization. Second, we introduce two ^{13}C-labeled residues, instead of one, in the same peptide, to enhance the signal-to-noise ratio. Third, we modify the search by releasing the con-

Received for publication 3 November 1998 and in final form 6 June 1999.
Address reprint requests to Dr. Isaiah T. Arkin, Biochemistry Department, Cambridge University, 80 Tennis Court Rd., Cambridge CB2 1GA, England. Tel.: 44-1223-766-048; Fax: 44-1223-766-002; E-mail: sa232@cam.ac.uk.

0006-3495/99/09/1594/08 $2.00

straint of the rotation angles and selecting the correct model from the pool of structures by subsequent analysis of the geometry. This extension is necessary because the low tilt of the *vpu* helices does not create substantial energy differences between models with different rotation angles for a specific residue.

The combined spectroscopic and molecular modeling approach yields in this case a single pentameric structure, which answers the question of *vpu* oligomerization and gives a detailed molecular structure of the transmembrane domain of the protein.

MATERIALS AND METHODS

Peptide purification and reconstitution

Synthetic peptides corresponding to the N-terminal domain of the HIV-1 *vpu* sequence found in different isolates (BH10, HXB3, MCK) (OWL composite database, version 30.02, 1998) were made by standard solid-phase F-moc chemistry, cleaved from the resin with trifluoroacetic acid, and lyophilized. The sequences corresponding to residues 1–31 are 1) MQPIQIAIVALVV $^{13}C_1$-AIIIAIV $^{13}C_1$-VWSIVIIEYRK and 2) MQPIQI-AIVALVVA $^{13}C_1$-IIIAIVV $^{13}C_1$-WSIVIIEYRK, each with two carbonyl ^{13}C amino acids (Cambridge Isotopes Laboratories, Andover, MA) at positions Val^{13}, Val^{20} and at positions Ala^{14}, Val^{21}, respectively. After the lyophilized peptides were dissolved in 2 ml of trifluoroacetic acid (final concentration ~5 mg/ml), they were injected into a 20-ml Jupiter 5C4-300 Å column (Phenomenex, Cheshire, England) equilibrated with 95% H_2O, 2% (w/v) acetonitrile, and 3% (v/v) 2-propanol. Peptide elution was achieved with a linear gradient to a final solvent composition of 5% H_2O, 20% trifluoroethanol, 28% acetonitrile, and 47% 2-propanol (Biocad Sprint; Perceptive Biosystems, Cambridge, MA). All solvents contained 0.1% (v/v) trifluoroacetic acid. Peptide-containing fractions were checked by mass spectrometry, and the pooled fractions were lyophilized and dissolved in a solution of 5% (w/v) β-octylglycopyranoside (Melford Laboratories, Ipswich, England) and 12.5 mg/ml dimyristoylphosphocholine (Sigma). After 24 h of dialysis in water, 6 h of dialysis in 10 mM phosphate $K_2HPO_4 \cdot KH_2PO_4$ buffer (pH 7.0) was performed.

Infrared spectroscopy

FTIR spectra were recorded on a Nicolet Magna 560 spectrometer (Madison, WI) equipped with a high-sensitivity liquid nitrogen-cooled MCT/A detector. Attenuated total reflection (ATR) spectra were measured with a 25-reflection ATR accessory from Graseby Specac (Kent, England) and a wire grid polarizer (0.25 μM; Graseby Specac). Two hundred microliters of sample (~2.5 mg/ml protein and 12.5 mg/ml lipid) were dried onto a trapezoidal Ge internal reflection element (50 × 2 × 20 mm) under a stream of nitrogen. After the instrument was extensively purged with dry nitrogen, 1000 interferograms were averaged for every sample and processed with 1-point zero filling Happ-Genzel apodization.

Fourier self-deconvolution (FSD) (Kauppinen et al., 1982) was applied to the spectra in the amide I region to separate the overlapping ^{12}C and isotope shifted ^{13}C (Tadesse et al., 1991) amide I peaks. The enhancement factor used in FSD was 2.0, and the half-height bandwidth was 13 cm^{-1}, as reported previously (Byler and Susi, 1986). The peaks were integrated after FSD in the regions 1670–1645 cm^{-1} and 1610–1630 cm^{-1} for the helix (^{12}C) and the site-specific label (^{13}C), respectively. The dichroic ratio $\mathcal{R}$ was calculated as the ratio between the integrated absorption of parallel and perpendicular polarized light. The site-specific dichroism $\mathcal{R}_{site}$ was corrected for the natural abundance of ^{13}C by the equation

$$\mathcal{R}_{site}^{corr} = \frac{\mathcal{R}_{helix}\mathcal{R}_{site}}{\mathcal{R}_{helix} + r(\mathcal{R}_{helix} - \mathcal{R}_{site})}, \quad (1)$$

where $\mathcal{R}_{helix}$ and $\mathcal{R}_{site}$ are dichroic ratios for the helix (^{12}C) and the site-specific (^{13}C) amide I mode, respectively, and r = 0.091 denotes the fraction of randomized ^{13}C in the 22-residue transmembrane part, considering the 1% natural abundance of ^{13}C. For transmission spectra, 50 μl of sample was dried on a CaF_2 window of 15 mm diameter. D_2O exchange was performed by incubating the sample for 2 h in 99% D_2O before drying. To monitor the D_2O exchange, the amide II band between 1525 cm^{-1} and 1570 cm^{-1} was integrated, and the area A_{II} was divided by the total amide I area ($y = A_{II}/A_I$) to account for differences in protein concentration. The amount of D_2O exchange was then calculated by dividing the corrected amide II area in D_2O (y_{D_2O}) by y_{H_2O}.

Data analysis

The data were analyzed according to the theory of site-specific dichroism presented in detail elsewhere (Arkin et al., 1997), with the extensions described in Kukol et al. (1999). Briefly, the measured dichroism, the absorption ratio $\mathcal{R}$, between parallel and perpendicular polarized light $\mathcal{R} = A_\parallel/A_\perp$, of a particular transition dipole moment is a function of its spatial orientation. For the amide I mode of an α-helical protein the geometric relation between the transition dipole moment (mainly the C═O bond) and the helix is known from fiber diffraction studies (Tsuboi, 1962). Therefore, by measuring the orientation of the amide I transition dipole one can determine the helix tilt angle β and the rotational pitch angle ω of the specific dipole moment about the helix axis. The rotational pitch angle ω is arbitrarily defined as 0° when the transition dipole moment, the helix director, and the *z* axis all reside in a single plane. Thus, measuring the site-specific dichroism $\mathcal{R}_{site}$ of the ^{13}C amide I mode at a particular label and the helix dichroism $\mathcal{R}_{helix}$ allows calculation of the helix tilt β and the rotational pitch angle ω of a particular label, as detailed by Arkin et al. (1997), if measurements from two samples with labels at different ω are analyzed together. Note that the difference in ω between two consecutive residues is assumed to be 100°, as in a standard α-helix. To enhance the ^{13}C amide I mode intensity we extend the formerly presented method by introducing two labels at positions i and $i + 7$. These two labels have approximately the same rotational pitch angle $\omega_i \approx \omega_{i+7}$ in α-helical geometry (Pauling et al., 1951). The error introduced in this assumption is compensated for by the fact that the signal of ^{13}C amide I mode is enhanced.

Molecular modeling

A global search with respect to rotation about the helix axis, assuming multimeric symmetry, was carried out as described in detail elsewhere (Adams et al., 1995). In brief, all calculations were performed with the parallel processing version of the Crystallography and NMR System (CNS Version 0.3) (Brunger et al., 1998). We have used the OPLS parameter set with a united atom topology, which explicitly represents the polar hydrogen and aromatic side-chain atoms (Jorgensen and Tirado-Rives, 1988). All calculations were carried out in vacuo with the initial coordinates of a canonical α-helix (3.6 residues per turn). Symmetric tetramers, pentamers, and hexamers (n = 4, 5, 6) were generated from the sequence IAIVALV-VAIIIAIVVWSIVII by replicating the helix and rotating it by 360°/n around the center of the multimer. The transmembrane sequence was predicted on the basis of hydropathy analysis. An initial crossing angle of 25° for left-handed and −25° for right-handed structures was introduced by rotating the long helix axis with respect to the long bundle axis. The symmetrical search was carried out by applying a rotation to all helices simultaneously between $\phi = 0°$ and $\phi = 360°$ in 10° steps. Four trials were carried out for each starting structure, using different initial random atom velocities in each case at both right- and left-handed crossing angles, yielding 36 × 4 × 2 = 288 structures. Each structure was subjected to a simulated annealing and energy minimization protocol. Clusters of similar structures were defined such that the root mean square deviation (RMSD) of the coordinates between two structures within a cluster was not larger than 1.0 Å; a cluster was formed by a minimum of 10 structures. For each

cluster an average structure was calculated, energy minimized, and then subjected to the same simulated annealing protocol as used in the systematic search.

Orientation refinement

To take into account the results obtained from the site-directed dichroism analysis, we have incorporated a new orientation refinement energy term in all molecular dynamics and energy minimization calculations:

$$E = k_{\text{dichro}}(\theta - \theta_0)^2 \tag{2}$$

where θ represents the actual angle and θ_0 the target angle. The overall weight constant k_{dichro} for these orientational constraints was chosen to be $k_{\text{dichro}} = 800$ kcal/rad^2, determined empirically by selecting the minimum value necessary to obtain an identical outcome from MD protocols with different constants. According to the experimental data, two different kinds of restraints can be applied (see Fig. 1):

A helix tilt restraint is applied by defining a vector connecting every C_α of residue i and C_α of residue $i + 7$. The angle between these vectors and the z axis is then set to the value obtained for the helix tilt (the angle β).

The four site-specific dichroism restraints are applied by setting the target angles θ between the corresponding ^{13}C═O bonds of Val^{13}, Val^{20}, Ala^{14}, and Val^{21} and the z axis to that obtained from the experiment. These angles are a function of the helix tilt β, the rotational pitch angle ω (Arkin et al., 1997), and the angle between the transition dipole moment and the helix director, which is known from fiber diffraction studies (Tsuboi, 1962) to be 39° and is $\alpha = 180° - 39° = 141°$, according to our definition:

$$\theta = 180° - \arccos(\cos\alpha\cos\beta - \sin\alpha\cos\omega\sin\beta) - 17° \tag{3}$$

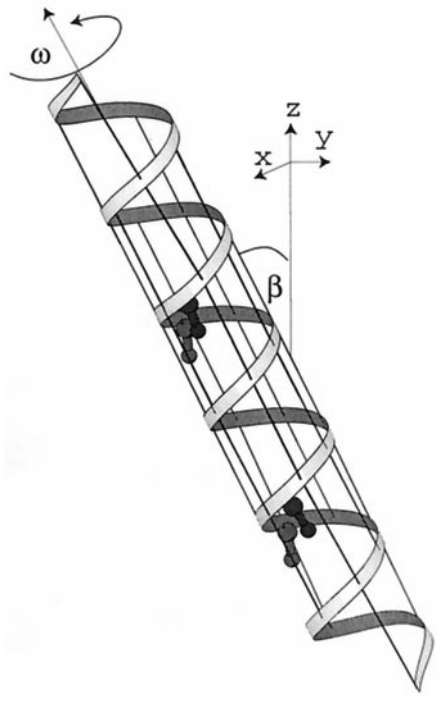

FIGURE 1 Schematic diagram of the orientational restraints employed during the molecular dynamics and energy minimization calculations. The helix tilt was restrained to the angle β by defining a vector between every C_α of residue i and C_α of residue $i + 7$, shown as lines. The C═O bonds of the labeled residue pair Val^{13}, Val^{20} and the residue pair Ala^{14}, Val^{21} are also shown.

To account for the angle difference between the C═O bond and the amide I transition dipole moment, 17° has to be subtracted (Tsuboi, 1962). We carried out the simulations with application of both restraints, with the helix tilt restraint only, and without restraints. The rotational pitch angles of the resulting structures were determined from a geometric analysis with a self-written program.

Interaction energy

The average interaction energy per residue gives the nonbonded interaction energy of a particular residue on one helix monomer with all other residues on all other helices.

RESULTS AND DISCUSSION

Secondary structure and membrane incorporation

Transmission FTIR spectra of the amide I and amide II regions of the *vpu* peptide reconstituted in lipid vesicles are shown in Fig. 2. From the dominant amide I intensity centered at 1655 cm^{-1} with a half-maximum peak width of 18 cm^{-1} (in H_2O), it can be concluded that the peptide is mostly α-helical (Braiman and Rothschild, 1988). The peak centered at 1615 cm^{-1} arises from the ^{13}C-labeled amino acids (Tadesse et al., 1991). Other contributions arise from the extramembranous part of the peptide, which contains 29% of the total amino acids.

The measurement of the amount of deuterium exchange after a period of 2 h, obtained by integration of the amide II area between 1525 cm^{-1} and 1555 cm^{-1} (see Fig. 2), gives a 46 ± 7% exchange, more than is expected from the 29% extramembranous portion. The results did not change after 6 h of incubation. Thus in addition to the extramembranous part, (24 ± 10)% of the transmembrane amide protons exchange with D_2O. This corresponds to 5 ± 2 amino acid residues that are accessible from the solution. This result can be discussed in terms of the question of ion channel formation by *vpu* (see below).

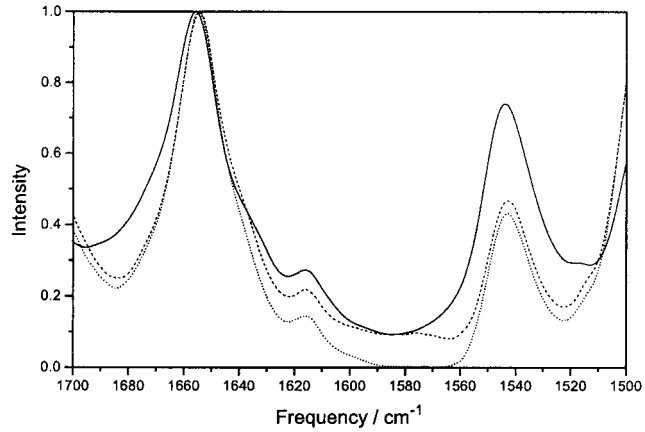

FIGURE 2 Transmission FTIR spectra of the amide I and amide II area of the Val^{13}/Val^{20} labeled *vpu* peptide in H_2O (—), after 2 h of incubation in D_2O (– – –), and after 6 h of incubation in D_2O (· · · · ·). The intensity is normalized to the amide I peak maximum.

Transmembrane orientation

It can be seen that the double-labeled ^{13}C samples result in a clearly observable amide I ^{13}C intensity, even without Fourier self-deconvolution (Fig. 3). The helix- and site-specific dichroisms (Table 1) obtained from the ATR spectra, as shown in Fig. 3, are similar. The quantitative analysis of the dichroism proceeds by combining each measurement of a sample with the label in position Val^{13}/Val^{20} and each measurement with the label in position Ala^{14}/Val^{21}, yielding 30 different pairwise results. The final average of the helix tilt is $\beta = (6.5 \pm 1.7)°$, and the rotational pitch angle is $\omega = (283 \pm 11)°$ for Val^{13}/Val^{20}. From these values the angle between the C═O bond and the z axis can be calculated with Eq. 3. The angles are 21° and 16° for Val^{13}/Val^{20} and Ala^{14}/Val^{21}, respectively.

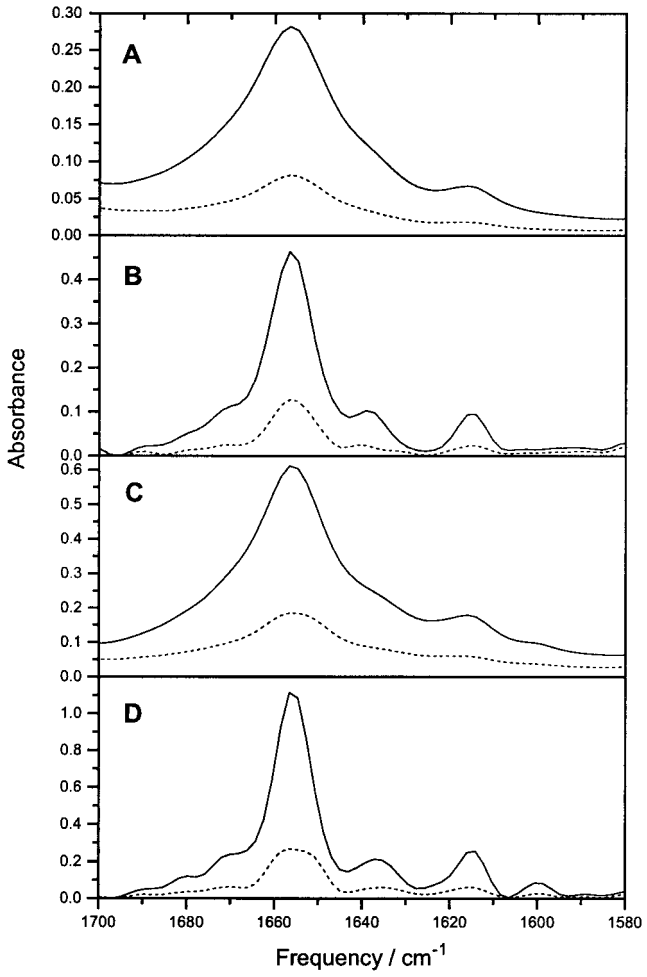

FIGURE 3 ATR-FTIR spectra of the lipid-vesicle reconstituted transmembrane domain of *vpu* in the amide I region obtained with parallel (—) and perpendicular (·····) polarized light. (*A* and *C*) Spectra of ^{13}C-labeled Val^{13}/Val^{20} and Ala^{14}/Val^{21}, respectively. (*B* and *D*) Fourier-self deconvoluted spectra of *A* and *C*.

Molecular model of the *vpu* transmembrane domain

Assuming tetrameric, pentameric, and hexameric oligomerization, 288 structures have been calculated for each oligomerization state by incrementing the helix rotation parameter ϕ in steps of 10°. Three different search protocols were used: 1) no experimental restraints were applied, 2) the helix tilt restraint was applied, 3) both helix tilt restraint and site-specific rotational restraints were applied. Upon the application of both restraints, no final cluster of structures could be found, based on the criteria of maximum number of structures forming a cluster and lowest energy of the average structure (data not shown). We have therefore performed the same search protocol without constraining the angle between the C═O bond and the z axis. Because this angle is a function of both the helix tilt β and the rotational pitch angle ω, removing this constraint generates structures, where the rotational pitch angle is not fixed at the experimental value. The parameters of the average cluster structures after energy minimization are given in Table 2. Inspection of the rotational pitch angles in Table 2 shows that pentamer structure 7 with $\omega_{Val13} = 316°$ has the rotational pitch angle closest to the experimental value, $\omega = (283 \pm 11)°$. Comparison of the energy of this structure, $E = -182$ kcal/mol^{-1}, with the other pentamer structures shows that it is also among the lowest energy structures. But only the experimentally determined pitch angle is used to choose this structure as a model of the *vpu* transmembrane domain.

Fig. 4 shows the structure of the *vpu* transmembrane domain. It is notable that the residue Trp^{22} is pointing into the channel lumen, thus occluding the pore, as can be seen in Fig. 5. The only hydrophilic residue, Ser^{23}, is pointing outward to the lipid phase, whereby the hydroxyl group is hydrogen-bonded to the carbonyl backbone atoms. Fig. 5 reveals that the pore is accessible up to Trp^{22}. The average interaction energy per residue is shown in Fig. 6. The periodicity of the maxima in this graph represents the periodicity of the helix, whereby Trp^{22} contributes most to the interaction energy.

Biological implications

The assumption that *vpu* forms ion channels is controversially discussed in the literature. In fact there is experimental evidence that low-level expression of *vpu* reduces membrane conductance in *Xenopus* oocytes (Coady et al., 1998). In the same study it is questioned that conventional oocyte expression studies are the appropriate method for addressing the formation of ion channels by *vpu*, because the amount of *vpu* mRNA (46 ng) often used is lethal within 2 days (Coady et al., 1998). However, conductance measurements in artificial lipid bilayers can be used to show the formation of ion channels. The single-channel traces of Schubert et al. (1996b), from planar bilayers, are clearly indicative of ion channel formation. But it remains unclear why the authors apparently introduced a Gln^2-Glu^2 muta-

TABLE 1 Helix dichroism $\mathcal{R}_{helix}$ and site-specific dichroism $\mathcal{R}_{site}$ and lipid asymmetric stretching modes $\mathcal{R}_{lipid}$ for the two *vpu* peptides as noted

Peptide	$\mathcal{R}_{helix}$	$\mathcal{R}_{site}$	$\mathcal{R}_{lipid}$	$\mathcal{S}_{lipid}$	β	ω
Val^{13}/Val^{20}	3.76 ± 0.13	4.01 ± 0.40	1.05 ± 0.06	0.507 ± 0.048	6.5° ± 1.7°	283° ± 11°
Val^{14}/Ala^{21}	3.44 ± 0.21	4.45 ± 0.47	1.15 ± 0.09	0.442 ± 0.068	6.5° ± 1.7°	23° ± 11°

Also shown are the calculated lipid order parameters $\mathcal{S}_{lipid} = (3\cos^2\beta - 1)/2$ (Braiman and Rothschild, 1988), the helix tilt angle β, and the rotational pitch angle ω about the helix axis.

tion in the synthetic *vpu* peptide that is not found in naturally occurring viral strains. The negative charge of deprotonated carboxylic acids may have a significant impact on ion channel function, even if they are located outside the membrane (e.g., Kukol and Neumann, 1998). The single-channel traces of Ewart et al. (1996) obtained with the wild-type *vpu* peptide are very noisy, and the conductance varies between 14 and 280 pS. Conductance measurements in lipid bilayers are sensitive to artifacts caused by aggregates of hydrophobic peptides (Tosteson et al., 1988), as pointed out by Coady et al. (1998). This could not be completely ruled out by looking at the data of Ewart et al. (1996). Our results provide some support for the ion channel hypothesis. Although the presented structure has a pore occluded by Trp residues, the deuterium exchange experiments, shown in Fig. 2, indicated that at least part of the transmembrane domain (5 ± 2 amino acid residues) is water accessible. This is compatible with the presence of a partially open pore like the one seen in Fig. 5. In this structure 16 amino acid residues are water accessible, as seen from the extracellular side. Thus the given structure may represent the closed conformation of an ion channel.

Limitations of the constrained MD search and site-directed infrared dichroism

The method of site-directed infrared dichroism has been applied to the *Influenza* M2 peptide (Kukol et al., 1999). In that instance it was possible, by introducing both the helix tilt and the rotational constraint, to obtain a unique model based on the criteria of lowest cluster energy and maximum

TABLE 2 Parameters of averaged structures obtained from the global search protocol, whereby only the helix tilt is constrained

Oligomerization	Structure no.	*E*/kcal/mol	No. of structures	Ω	ϕ	$\omega_{Val^{13}}$	$\omega_{Ala^{14}}$
Tetramer	1	−125	18	7.7°	32°	27°	130°
	2	−105	48	0.7°	79°	—	—
	3	−125	10	5.5°	139°	88°	195°
	4	−148	28	4.4°	196°	172°	231°
	5	−125	44	−1.1°	244°	0°	104°
	6	−139	19	2.3°	298°	—	—
	7	−91	20	−4.3°	12°	154°	255°
	8	−91	16	−1.3°	151°	26°	127°
	9	−127	20	−1.1°	187°	23°	121°
	10	−144	11	0°	302°	32°	126°
Pentamer	1	−145	17	4.0°	346°	0°	106°
	2	−184	13	7.2°	39°	40°	141°
	3	−144	32	4.5°	87°	66°	167°
	4	−157	15	4.9°	142°	95°	205°
	5	−187	20	5.0°	202°	121°	221°
	6	−153	32	−1.4°	253°	34°	135°
	7	−182	20	−5.5°	301°	316°	55°
	8	−103	32	−1.7°	16°	—	—
	9	−111	11	−6.4°	120°	334°	71°
	10	−160	15	−4.8°	313°	99°	203°
Hexamer	1	−160	10	7.6°	2.8°	34°	136°
	2	−161	16	4.4°	49°	68°	168°
	3	−164	10	4.8°	101°	90°	200°
	4	−195	13	4.8°	162°	131°	229°
	5	−161	26	−1.3°	214°	39°	140°
	6	−212	19	3.6°	257°	—	—
	7	−123	10	6.9°	304°	340°	83°
	8	−134	10	2.0°	337°	20°	120°
	9	−131	23	−2.0°	140°	20°	117°

The energy (*E*) of each structure, number of structures considered for the average, helix crossing angle Ω, helix rotation parameter ϕ, and rotational pitch angles $\omega_{Val^{13}}$, $\omega_{Ala^{14}}$ are given. The angles are averages over all helices of a structure. Dashes denote cases in which ω shows large variations between individual helices (more than 60°) and the average could not be determined.

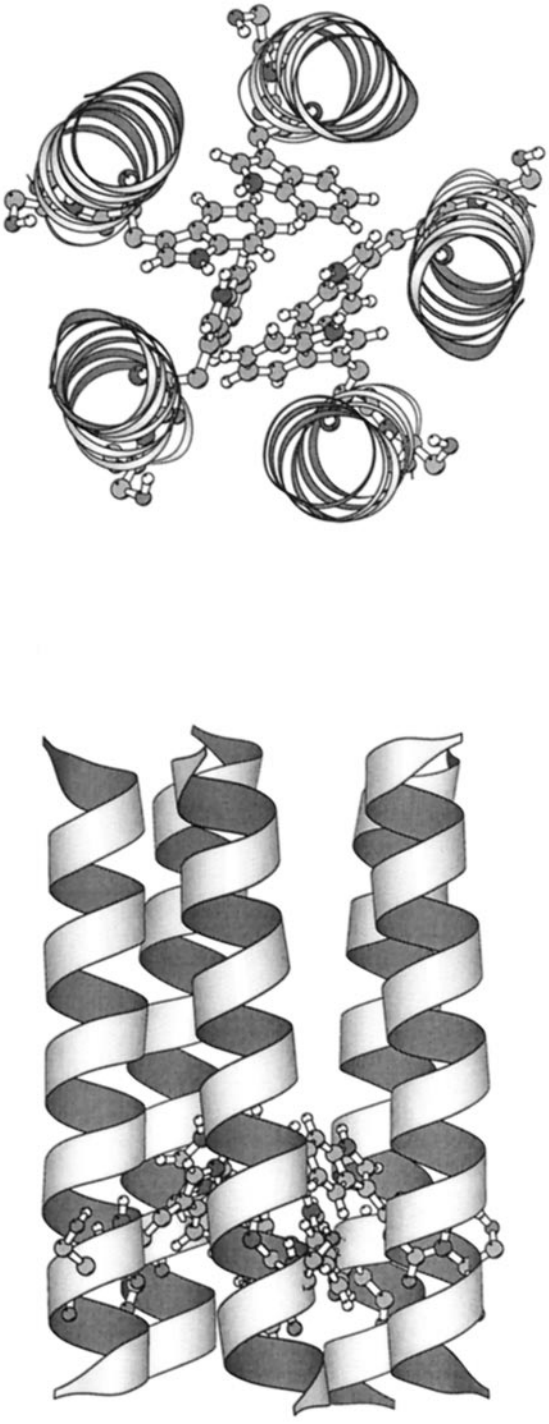

FIGURE 4 Ribbon diagrams of the *vpu* transmembrane structure, shown from the N-terminus from Ile^{6} to Ile^{27} (*top*) and from the side (*bottom*). The residues Trp^{22} and Ser^{23} are shown in a ball-and-stick display. The figure was created with Molscript (Kraulis, 1991).

number of structures converging to a single cluster. In our case, the unclear discrimination among the different structures according to the criteria of lowest energy and highest number of substructures forming a cluster is a result of the inherent low tilt angle β of the examined system. One of the experimental energy refinement terms employed during the

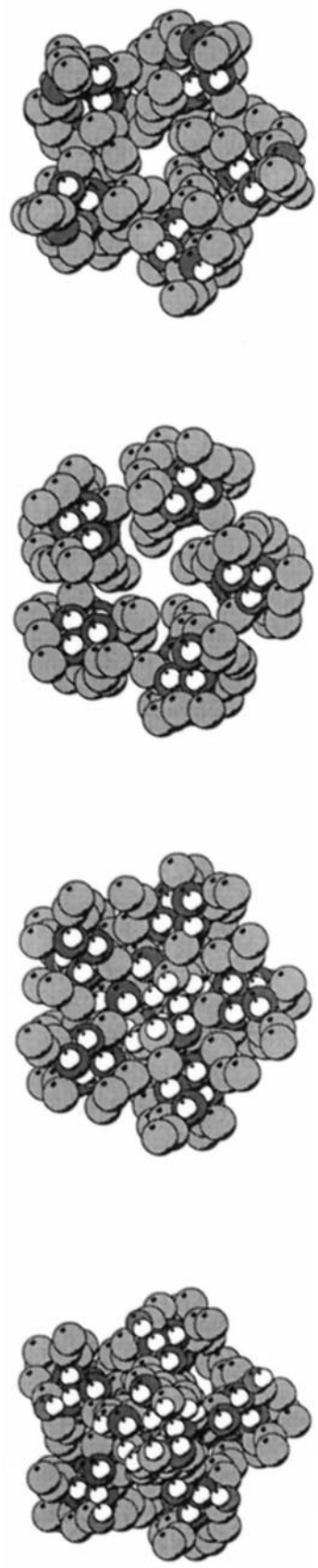

FIGURE 5 Slices of the *vpu* transmembrane structure. From top to bottom: Ile^{6}-Val^{12}, Val^{12}-Ile^{17}, Ile^{17}-Trp^{22}, and Trp^{22}-Ile^{27}. The figure was created with Molscript (Kraulis, 1991).

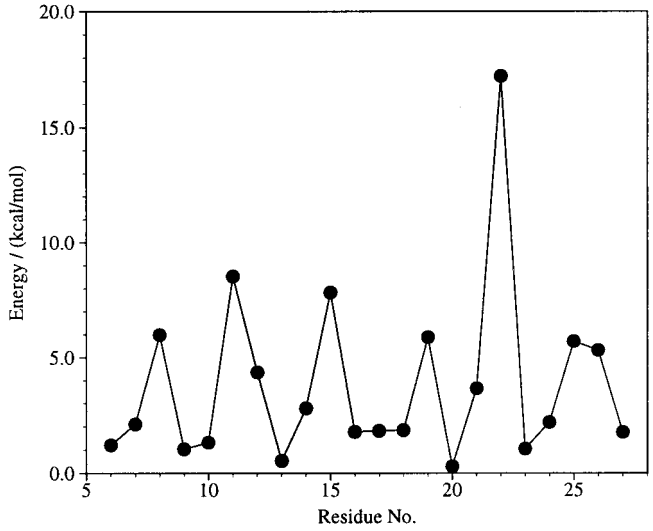

FIGURE 6 Interaction energy per residue, averaged from the five helices in the pentamer structure.

MD simulation is dependent on the angle θ between the C═O bond and the z axis, which is a function of the helix tilt β and rotational pitch angle ω of the specific residue. Thus inserting Eq. 3 into Eq. 2, one obtains

$$E = k_{\text{dichro}}((180^\circ - \arccos(\cos\alpha\cos\beta - \sin\alpha\cos\omega\sin\beta) - 17^\circ - \theta_0)^2 \quad (4)$$

This gives the refinement energy as a function of ω and β. By plotting Eq. 4 (Fig. 7) for different helix tilt angles β, it becomes apparent that the energetic discrimination among ω values is low at a tilt angle of $\beta = 6.5°$ compared to $\beta = 31°$, as obtained from the *Influenza* M2 peptide (Kukol et al., 1999).

Furthermore, the method of site-directed dichroism is limited to determining ω at low helix tilt angles. If the helix tilt angle is zero, the site-specific dichroism is equal to the

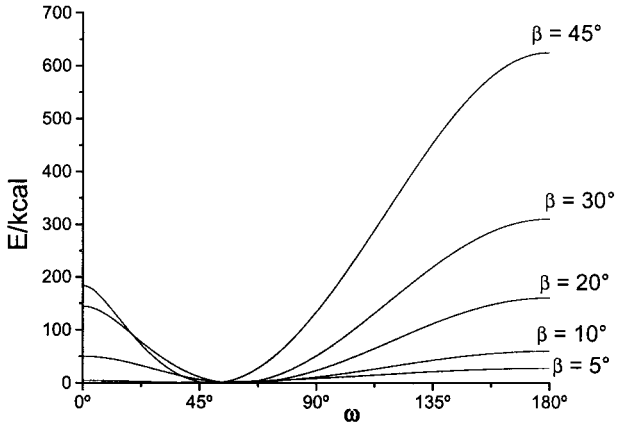

FIGURE 7 Dependence of the refinement energy term for the angle θ between the C═O bond and the z axis on the rotational pitch angle ω. Curves for different helix tilt angles β are shown as indicated. Calculated from Eq. 4, setting $\theta_0 = 21°$ and $k_{\text{dichro}} = 800$ kcal/grad^2.

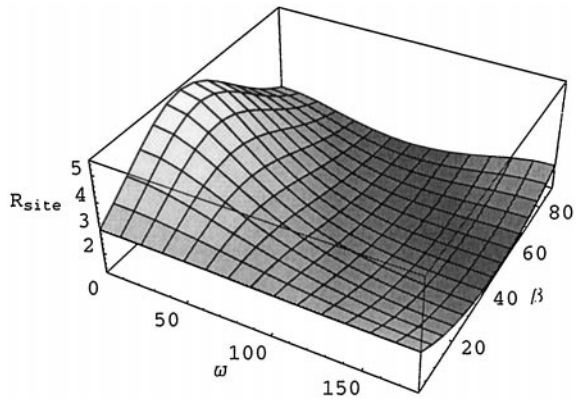

FIGURE 8 Dependence of the site-specific dichroism $\mathcal{R}_{\text{site}}$ on the rotational pitch angle ω and the helix tilt β. Calculated with equation 12 from Arkin et al. (1997).

helix dichroism and the rotational pitch angle ω cannot be obtained. This becomes apparent in Fig. 8, where the site-specific dichroism is plotted as a function of ω and the helix tilt β. The difference in the site-specific dichroism is at maximum for different ω when the helix is tilted by 45°. In our case ω has been obtained from the averaging of 30 different results. This allows the determination of ω to a reasonable accuracy and the subsequent selection of structures that correspond to the experimentally derived angle.

The same limitations also apply to orientational constraints derived from solid-state NMR spectroscopy, which have been recently obtained for the *Influenza* M2 peptide (Kovacs and Cross, 1997).

CONCLUSIONS

It has been shown that the transmembrane part of the HIV-1 *vpu* peptide forms an α-helical structure in a lipid environment, where the helices are tilted by $\beta = (6.5 \pm 1.7)°$ and the rotational pitch angle of Val^{13} is $\omega = (283 \pm 11)°$. A molecular modeling approach including the experimental data gave a pentameric structure of the *vpu* peptide, although the oligomerization state was not known a priori. This structure forms the basis for further investigations by biophysical techniques.

We are indebted to Paul D. Adams, the Howard Hughes Medical Institute, and the Department of Molecular Biophysics, Yale University, for providing the helical search routines. We thank Prof. Dennis Pederson and Dr. Jaume Torres for carefully reading the manuscript and Tim Stevens for developing the word count program.

This work was supported by grants from the Welcome Trust and the BBSRC.

REFERENCES

Adams, P., I. Arkin, D. Engelman, and A. Brunger. 1995. Computational searching and mutagenesis suggests a structure for the pentameric transmembrane domain of phospholamban. *Nature Struct Biol.* 2:154–162.

Arkin, I., K. MacKenzie, and A. Brunger. 1997. Site-directed dichroism as a method for obtaining rotational and orientational constraints for oriented polymers. *J. Am. Chem. Soc.* 119:8973–8190.

Braiman, M., and K. Rothschild. 1988. Fourier transform infrared techniques for probing membrane protein structure. *Annu. Rev. Biophys. Biophys. Chem.* 17:541–570.

Brunger, A., P. Adams, G. Clore, W. Gros, R. Grosse-Kunstleve, J. Jiang, J. Kuszewski, M. Nilges, N. Pannu, R. Read, L. Rice, T. Simonson, and G. Warren. 1998. Crystallography and NMR system: a new software suite for macromolecular structure determination. *Acta Crystallogr. D Biol. Crystallogr.* 54:905–921.

Byler, D., and H. Susi. 1986. Examination of the secondary structure of proteins by deconvolved FTIR spectra. *Biopolymers.* 25:469–487.

Cladera, J., J. Torres, and E. Padros. 1996. Analysis of conformational changes in bacteriorhodopsin upon retinal removal. *Biophys. J.* 70: 2882–2887.

Coady, M., N. Daniel, E. Tiganos, B. Allain, J. Friborg, J.-Y. Lapointe, and E. Cohen. 1998. Effects of vpu expression on *Xenopus* oocyte membrane conductance. *Virology.* 244:39–49.

Cohen, E., E. Terwilliger, J. Sodroski, and W. Haseltine. 1988. Identification of a protein encoded by the vpu gene of HIV-1. *Nature.* 334: 532–534.

Ewart, G., T. Sutherland, P. Gage, and G. Cox. 1996. The Vpu protein of human immunodeficiency virus type 1 forms cation-selective ion channels. *J. Virol.* 70:7108–7115.

Friborg, J., A. Ladha, H. Gottlinger, W. Haseltine, and E. Cohen. 1995. Functional analysis of the phosphorylation sites on the human immunodeficiency virus type 1 Vpu protein. *J. Acquir. Immune Defic. Syndr.* 8:10–22.

Gonzales, M., and L. Carrasco. 1998. The human immunodeficiency virus type I Vpu protein enhances membrane permeability. *Biochemistry.* 37:13710–13719.

Gottlinger, H., T. Dorfman, E. Cohen, and W. Haseltine. 1993. Vpu protein of human immunodeficiency virus type 1 enhances the release of capsids produced by gag gene constructs of widely divergent retroviruses. *Proc. Natl. Acad. Sci. USA.* 90:7381–7385.

Holsinger, L., D. Nichani, L. Pinto, and R. Lamb. 1994. Influenza A virus M2 ion channel protein: a structure-function analysis. *J. Virol.* 68: 1551–1563.

Jorgensen, W., and J. Tirado-Rives. 1988. The OPLS potential function for proteins, energy minimization for crystals of cyclic peptides and crambin? *J. Am. Chem. Soc.* 110:1657–1666.

Kauppinen, J., D. Moffatt, H. Mantsch, and D. Cameron. 1982. Fourier self-deconvolution: a method for resolving intrinsically overlapped bands. *Appl. Spectrosc.* 35:271–276.

Klimkait, T., K. Strebel, M. Hoggan, M. Martin, and J. Orenstein. 1990. The human immunodeficiency virus type 1-specific protein vpu is required for efficient virus maturation and release. *J. Virol.* 64:621–629.

Kovacs, F., and T. Cross. 1997. Transmembrane four-helix bundle of *Influenza* A M2 protein channel: structural implications from helix tilt and orientation. *Biophys. J.* 73:2511–2517.

Kraulis, P. 1991. Molscript: a program to produce both detailed and schematic plots of protein structures. *J. Appl. Crystallogr.* 24:946–950.

Kukol, A., P. Adams, A. Brunger, and I. Arkin. 1999. Experimental based spatial refinement of membrane protein models: a structure for the *Influenza* A M2-H+ channel. *J. Mol. Biol.* 286:951–962.

Kukol, A., and E. Neumann. 1998. Electrostatic determinants of the ion channel control of the nicotinic acetylcholine receptor of *Torpedo californica. Eur. Biophys. J.* 27:618–625.

Lamb, R., and L. Pinto. 1997. Do vpu and vpr of human immunodeficiency virus type 1 and nb of *Influenza* b virus have ion channel activities in the viral life cycles? *Virology.* 229:1–11.

Maldarelli, F., R. Willey, and K. Strebel. 1993. Human immunodeficiency virus type 1 Vpu protein is an oligomeric type I integral membrane protein. *J. Virol.* 67:5056–5061.

Pauling, L., R. Corey, and H. Branson. 1951. The structure of proteins: two hydrogen-bonded helical configurations of the polypeptide chain. *Proc. Natl. Acad. Sci. USA.* 37:205–211.

Sansom, M. 1998. Models and simulations of ion channels and related membrane proteins. *Curr. Opin. Struct. Biol.* 8:237–244.

Sansom, M., L. Forrest, and R. Bull. 1998. Viral ion channels: molecular modeling and simulation. *BioEssays.* 20:1–10.

Schubert, U., S. Bour, A. Ferrer-Montiel, M. Montal, and F. Maldarelli. 1996a. The two biological activities of human immunodeficiency virus type 1 Vpu protein involve two separable structural domains. *J. Virol.* 70:809–819.

Schubert, U., A. Ferrer-Montiel, M. Oblatt-Montal, P. Henklein, K. Strebel, and M. Montal. 1996b. Identification of an ion channel activity of the Vpu transmembrane domain and its involvement in the regulation of virus release from HIV-1-infected cells. *FEBS Lett.* 398:12–18.

Schubert, U., and K. Strebel. 1994. Differential activities of the human immunodeficiency virus type 1-encoded Vpu protein are regulated by phosphorylation and occur in different cellular compartments. *J. Virol.* 68:2260–2271.

Strebel, K., T. Klimkait, F. Maldarelli, and M. Martin. 1989. Molecular and biochemical analyses of human immunodeficiency virus type 1 vpu protein. *J. Virol.* 63:3784–3791.

Strebel, K., T. Klimkait, and M. Martin. 1988. A novel gene of HIV-1, vpu, and its 16-kilodalton product. *Science.* 241:1221–1223.

Tadesse, L., R. Nazarbaghi, and L. Walters. 1991. Isotopically enhanced infrared spectroscopy: a novel method for examining the secondary structure at specific sites in conformationally heterogenous peptides. *J. Am. Chem. Soc.* 113:7036–7037.

Torres, J., J. Sepulcre, and E. Padros. 1995. Conformational changes in bacteriorhodopsin associated with protein-protein interactions: a functional alpha(I)-alpha(II) helix switch. *Biochemistry.* 34:16320–16326.

Tosteson, M., M. Caulfield, J. Levy, M. Rosenblatt, and D. Tosteson. 1988. The synthetic precursor specific region of pre-proparathyroid hormone forms ion channels in lipid bilayers. *Biosci. Rep.* 8:173–183.

Tsuboi, M. 1962. Infrared dichroism and molecular conformation of a-form poly-γ-benzyl-L-glutamate. *J. Polym. Sci.* 59:139–153.

Xiao Jian, Y., H. Gottlinger, W. Haseltine, and E. Cohen. 1992. Envelope glycoprotein and CD4 independence of vpu-facilitated human immunodeficiency virus type 1 capsid export. *J. Virol.* 66:5119–5126.